PPPL-3183 - Preprint: May 1996, UC-420, 424, 426

Fusion Reactivity, Confinement, and Stability of Neutral-Beam Heated Plasmas in TFTR and other Tokamaks*

Hyeon K. Park
Princeton Plasma Physics Laboratory, Princeton University, Princeton, NJ 08543

Steven A. Sabbagh†
Department of Applied Physics, Columbia University, New York, NY 10027

ABSTRACT

The hypothesis that the heating beam fueling profile shape connects the edge condition and improved core confinement and fusion reactivity is extensively studied on TFTR and applied to other tokamaks. The derived absolute scalings [Ref. 3] based on beam fueling profile shape for the stored energy and neutron yield can be applied to the deuterium discharges at different major radii in TFTR. These include Supershot, High poloidal beta, L-mode, and discharges with a reversed shear (RS) magnetic configuration. These scalings are also applied to deuterium-tritium discharges. The role of plasma parameters, such as plasma current, Isdo2(p), edge safety factor, *qsdo5(a*), and toroidal field, Bsdo2(T), in the performance and stability of the discharges is explicitly studied. Based on practical and externally controllable plasma parameters, the limitation and optimization of fusion power production of the present TFTR is investigated and a path for a discharge condition with fusion power gain, $Q > 1$ is suggested based on this study. Similar physics interpretation is provided for beam heated discharges on other major tokamaks.

1. INTRODUCTION

Following the "Supershot" experiment [1] on the Tokamak Fusion Test Reactor (TFTR), among other improved confinement characteristics, high ion temperature [Tsdo2(i)(0) > Tsdo2(e)(0)] leads to significantly enhanced fusion reactivity and energy confinement. Similar regimes have been observed in most large tokamaks. On TFTR, the role of plasma edge conditions modified by various wall conditioning techniques has been the key to obtaining "Supershots". As shown in Fig. 1, the measured global energy confinement time at the maximum stored energy is well anti-correlated with the edge parameters [2] such as an edge density, Csup2(+2), and Hsdo2(a) emission at a fixed plasma size. At the same time, the beam fueling parameter shows an excellent correlation with the measured energy confinement time. There are presently many different theories under study to explain the increase in τσδο2(E), such as the ITG mode, trapped electron mode, shear of magnetic field and/or velocity and many others. This paper focusses on the global empirical study based on the beam fueling parameter which connects the core improvement with the change of edge conditions.

The peak stored energy and neutron yields have been described by self-consistent scalings [3] based on the heating beam-fueling profile [4] in discharges dominated by neutral beam heating in TFTR. The study showed that the beam fueling profile affects the energy confinement of ions and electrons in vastly different ways. It is shown that the derived scalings [3] can be applied to all beam heated deuterium (D) discharges in TFTR such as L-mode discharges (whose confinement times fit the empirical L-mode scalings [5, 6]), the Supershot [1], High poloidal beta plasmas [7], discharges with a reversed shear (RS) magnetic configuration [8], and Supershots enhanced by Li pellet conditioning [9, 10]. When these scalings were applied to deuterium-tritium (DT) discharges, the stored energy scaling needed a mutiplier (~1.25) comparable to the result of an "isotopic effect" [11]. From the neutron scaling, one can estimate a reliable scale factor between D and DT neutron yields.

It is explicitly demonstrated that the global performance of a discharge (stored energy and fusion reactivity) is heavily dependent upon the core fueling of the heating beams . The plasma param-

eters such as plasma current, toroidal field, and the pressure and current profile peakedness are important in the determination of both the central and global β-limits. Based on practical and externally controllable plasma parameters, it can be shown that an important limitation to fusion production in the present TFTR is due to a central β-limit and a possible path to discharges with fusion power gain, Q > 1 can be suggested. Furthermore, a similar physics basis can be introduced to interpret beam heated discharges in other major tokamaks.

In section II, a review of the role of the neutral-beam fueling profile shape factor (Hsdo2(ne)) in determining the stored energy of each plasma species (ions and electrons) and the D fusion neutron emission is provided. It is also demonstrated that the two scalings (stored energy and neutron yields) are self-consistent. In section III, further tests of the derived scalings for D discharges at different major radii, and DT discharges are discussed. Here, it is shown that the neutron production of discharges is not directly influenced by the plasma current, edge safety factor, and toroidal field within the stability boundary where MHD activity is moderate [12].

In Section IV, the operating boundary of the TFTR experiment with respect to stability limits is discussed emphasizing the importance of plasma current and toroidal field in determination of the central as well as the global β-limits. It is demonstrated that the conventional Troyon limit can be modified to accomodate disruptions at extremely low βsdo2(N). In Section V, an operational fusion power diagram based on controllable external parameters together with stabiliy limits is compared to DT experimental results. Based on these results, it is conceivable that a tokamak can be designed in a regime with Q > 1 with present technology. In section VI, a similar physics basis is attempted to interpret the published literature and on-going research on neutral beam heated plasmas in other tokamaks (DIII-D, TEXTOR, JET, JT60-U).

2. REVIEW OF THE SCALINGS FOR ENERGY CONFINEMENT AND NEUTRON YIELD

a) Heating Beam Fueling Profile

The definition as well as the detailed calculation of the computed neutral-beam particle deposition profile shape factor, Hsdo2(ne), for TFTR are provided in Ref. [3,4]. Following these studies, Hsdo2(ne) is defined as

$$Hsdo2(ne) = f(Ssdo2(be)(0,t), \langle Ssdo2(be)(r,t) \rangle) \quad , \qquad [1]$$

where Ssdo2(be)(0,t) and <Ssdo2(be)(r,t)> are the central and volume-averaged electron source rates due to the neutral-beam, respectively. This definition is similar to the density peakedness factor Fsdo2(ne)=nsdo2(e)(0)/<nsdo2(e)>, where nsdo2(e)(0) is the central electron density and <nsdo2(e)> is volume-averaged electron density. The attenuation of the injected neutral-beam is to first order proportional to the local electron density, so a peaked neutral-beam deposition profile can be achieved at high density only with a peaked density profile. In order to parameterize the expression of Hsdo2(ne) for a variety of discharges, a regression has been performed for values of Hsdo2(ne) calculated by the TRANSP code [13] as a function of line-averaged electron density and the density peakedness factor. Among the functional combinations, the best description is

$$Hsdo2(ne) \propto Fsdo2(1.05,ne)EXP(-0.24\ nsdo2(e)), \qquad [2]$$

where Fsdo2(ne) and nsdo2(e) are the measured peakedness and line-averaged density of electrons. The relationship in Eq. [2] shows that a peaked electron density profile shape is essential for peaked deposition of the neutral-beam at high density. This expression with the same coefficients is applicable to TFTR discharges at different major radius discussed in this paper.

The fact that the derived beam-fueling profile [Eq. 2] on TFTR is sensitive to both the profile shape (Fsdo2(ne)) and magnitude of the electron density (in this case, the beam sources are said to be

"marginal") largely explains the observed characteristics of Supershot discharges; low edge density due to an intense wall conditioning and peaked central density due to efficient central beam fueling. The same explanation can be given for the results of density perturbation experiments in Supershots [14, 15]. In these experiments, Supershot discharges are perturbed by gas and/or pellet injection and the global confinement time degrades rapidly to the L-mode regime. Considering the fact that the rise of the edge density (an increase of line-averaged density and reduction of peakedness) due to the gas and/or pellet injection can reduce the central beam fueling, degradation of ion confinement is inevitable if the hypothesis that the ion stored energy is strongly correlated with the central beam fueling is correct. A recent significant improvement in energy confinement and neutron production created by intense wall conditioning using Li-pellet injection [10] is yet another excellent example that supports this hypothesis.

Among other distinctive characteristics, the performance of beam-heated discharges in TFTR has been strongly correlated with the peakedness of the electron density profile [16]. Although there has been an attempt to interpret the observed correlation with the transport physics associated with the density gradient, the results were not conclusive [17]. However, it is important to note that a peaked electron density profile alone is not a sufficient condition to improve the stored plasma energy in beam heated discharges in TFTR. As explained in Ref. 3, using pellets to fuel TFTR plasmas to high density does not result in enhanced confinement. This result is consistent with the corresponding exponential decrease of Hsdo2(ne) [Eq. 2] at sufficiently high density.

Due to the diagnostic difficulty of beam deposition or fueling profile measurement, obtaining these parameters has entirely relied upon modeling. One has to be extremely careful in the modeling of these parameters. It requires accurate information on beam sources such as divergence, energy components, impurities, cross-sections, and also the plasma parameters. For example, the deuterium neutral beam source with a full energy of about 100 keV on TFTR actually has three different energy components. The full, half, and third energy species typically comprise 45%, 26%, and 29% of the beam, respectively. For a tritium neutral beam, the ratios are 51%, 24%, and 25% due to the improved neutral-

ization cross section in tritium. Even for fairly high density plasmas on TFTR, the full energy component can be deposited near the center, but the deposition of the half energy component is affected significantly by the variation of plasma density. In order to minimize complications of the physics analysis, it would be desirable to have a heating-beam source which does not have multi-energy species. For further simplicity, one needs a beam source which will minimize the interaction with the plasma density variation.

b) Energy confinement and neutron yield

In order to provide better insight into the energy confinement scaling, the energy content of the plasma is divided into two species (electrons and ions) in this study. The observed scatter in the ion stored energy data as the heating power is varied can be significantly reduced by the additional parameters Hsdo2(ne) and Isdo2(P). Most importantly, it has been shown in Ref. [3] that the role of Hsdo2(ne) is much more significant than that of Isdo2(p). Thus the stored ion energy can be described by Psdo2(B) and Hsdo2(ne) as shown in Fig. 2 with the scaling

$$\text{Wsdo2(i) (MJ)} = \text{Csdo2(1) Psdo(1.3,B)(MW)Hsdo2(0.8,ne)}, \quad [3]$$

where Csdo2(1) is 20383. The fact that the stored ion energy scaling is nearly linearly correlated with the central beam fueling (Psdo2(B)Hsdo2(ne)) is especially striking. If ion transport at the center of the plasma is subtantially decreased as the central fueling is increased, the stored ion energy is expected to have a correlation stronger than a nearly linear relationship. Likewise, the stored ion energy should be correlated with less than a linear dependence when transport is increased as the central fueling is increased.

On the other hand, the parameteric dependence of the electron stored energy is significantly different from that of the ion channel. The result is given as

$$Wsdo2(e)(MJ) = Csdo2(2)\ Psup2(0.7,B)(MW)\ Isup2(0.4,P)(A)\ ,$$

[4]

where Csdo2(2) is 313. While Hsdo2(ne) is important in the determination of the ion stored energy, it is not important in the determination of the electron stored energy. The total stored energy of beam heated discharges can be defined simply as

$$Wsdo2(P,tot) = Wsdo2(i) + Wsdo2(e).$$

[5]

In TFTR, the neutron emission rate, Ssdo2(n), from DD reactions has been strongly correlated with the ion stored energy ($Ssdo2(n) \propto Wsdo2(1.6,i)$) as shown in Fig. 3. This result can be understood based on the fundamental reaction argument. The fusion cross-section ($<\sigma v>$) is proportional to ~ Tsdo2(2,i) for the range of ion temperatures (10 keV ~30 keV) on TFTR. Since the neutron yield is not entirely due to the thermonuclear reaction, the dependence is expected to be less than square. Using the same set of independent parameters employed in the study of energy confinement, the scaling result for the fusion reactivity is

$$Ssdo2(P,n) = C\ Psdo2(2.2,B)(MW)\ Hsdo2(1.3,ne)/\ Vsdo2(p)(m)\ ,$$

[6]

where C is 2.71 x 10sup2(14) and Vsdo2(p) is plasma volume. The expression in Eq. [6] is consistent with the derived ion stored energy via the correlation between neutron yield and stored ion energy ($Ssdo2(n) \propto Wsdo2(1.6,i)$).

Furthermore, we can define the fusion power gain for DD discharges, Qsdo2(DD), for a fixed plasma volume as

$$Qsdo2(DD) = Ssdo2(P,n) / Psdo2(B) \propto C\ Psdo2(1.2,B)(MW)\ Hsdo2(1.3,ne)\ . \quad [7]$$

As shown in this equation, Qsdo2(DD) is nearly linear to the central beam fueling. However, it is most practical to improve Qsdo2(DD) by increasing Hsdo2(ne) for a given heating beam power. In practice, there are limitations to the indefinite increase of Hsdo2(ne). The practical constraints and control of Hsdo2(ne) will be discussed in section 5.

3. FURTHER APPLICATION OF THE SCALINGS ON TFTR

The scaling study of the previous section was based on discharges obtained at Rsdo2(0) = 2.45 m (Vsdo2(p) = 30 msup2(3)) with a conditioned carbon limiter. Since then, Supershot regime study has been extended to discharges at different major radius with various wall conditions. In order to assure that the tested hypothesis that the improved core performance accompanied with the change of edge conditioning can be explained by the beam fueling parameter, the derived absolute scalings can be applied for the discharges obtained with a different boundary conditions. It was shown clearly that the plasma current was not an important factor in the determination of the ion stored energy (dominant energy component) whereas the electron stored energy was rather sensitive to the plasma current (remnants of L-mode scaling). Since the plasma size is fixed and the variation of toroidal field is small (~ 20 %), one can expect that the stored energy of beam heated discharges is largely independent of the edge safety factor (*qsdo2(a)*) as shown in Fig. 4 [16].

As limiter conditioning techniques have been developed using lithium pellets [9, 10], most of the recent D and DT discharges were operated at a larger major radius (Rsdo2(0) = 2.52 m, Vsdo2(p) = 37 msup2(3)). This has produced enhanced Supershot discharges with energy confinement times up to ~330 msec [10]. Note that the high energy confinement time obtained with lithium wall conditioning is almost twice that of the highest energy confinement time of the data base studied. In addition to these

high performance discharges, an L-mode study was also recently performed with both D and DT plasmas with beam heated discharges at an even a larger major radius (Rsdo2(0) = 2.62 m, Vsdo2(p) = 46 msup2(3)). This data set includes discharges with a reversed shear (RS) magnetic configuration [8].

The measured stored energies for D discharges with monotonic q profiles obtained at three different major radii are illustrated as a function of the derived scalings [Eq. 6] in Fig. 5a. As shown in this figure, it is quite interesting that neither the major radius nor plasma volume is not needed to describe the stored energy of the beam heated discharges. However, one has to keep in mind that the geometric factors are folded in to the Hsdop2(ne) calculation. Fig. 5b illustrates that Supershot discharges as well as L-mode discharges are forced to fit the absolute scaling (Wsdo2(p,tot)). In addition, the discharges (~150 shots) with reversed shear (RS) magnetic configuration are also compared with Wsdo2(p,tot) which fits well with both L-mode and Supershot discharges. Note that the discharges with RS configuration fits well with 0.8 x Wsdo2(p,tot). When neutron production was examined for discharges with the RS configuration, the result was 0.65 x Ssdo2(p,n) which is consistent with the prediction based on the self-consistent relationship between neutron production and stored energy discussed in the previous section. The central beam fueling is exceptionally good for some discharges with RS configuration but the stored energy and fusion reactivity are well below the level of Supershot discharges if the same logistics on confinement and fusion reactivity are applied.

The initial DT experiments [18, 19] on TFTR, showed that the stored energy of DT discharges is about ~ 25% higher than that of comparable D discharges. This fact has been attributed to an "isotopic effect" [11] due to the usage of tritium. When the scaling (Wsdo2(p,tot)) of the stored energy derived from D discharges is applied to DT plasmas, it is found that the stored energy of DT discharges (both supershots and L-mode discharges) fits to 1.25 x Wsdo2(p,tot) as shown in Fig. 6a. Note that the DT discharges in this figure have a fuel ratio (T/(D+T)) ranging from 30% to 70%. The neutron yield in DT plasmas is compared with Ssdo2(p,n) in Fig. 6b. Considering that there are many differences between deuterium and tritium beam sources as discussed in section 2(a), it would be desirable to have a comparison study of ohmic deuterium and tritium plasmas where the energy of the neutral of D and T

are identical, in order to clarify whether or not this difference is due to an intrinsic "isotopic effect" in the plasma rather than an "isotopic effect" in the heating beam sources.

Another important application of the scalings can be a study of toroidal field dependence of the stored energy. The derived scaling for the stored energy does not have Bsdo2(T) as an independent parameter, since the variation of Bsdo2(T) was restricted within small ranges (<20 %). In the process of optimizing the fusion power in DT experiments, an extensive D experiment was carried out at different toroidal magnetic fields. The toroidal field was varied from up to 5.6 T. It is readily shown that the global stored energy is not effected by the variation of toroidal field in this range. In Fig. 7, the measured stored energy is compared to Wsdo2(p,tot) for many different toroidal fields. The ratio is anchored at discharges at Rsdo2(o)=2.45 m with Bsdo2(T)=4 T. The DT discharges are accounted the multiplier (1.25) compared to the D discharges.

4. STABILITY AND OPTIMIZED FUSION POWER PRODUCTION

Reaching greater levels of fusion power output in TFTR is presently limited not by plasma confinement, but rather by plasma stability. Since fusion reactivity scales approximately as $\beta\sigma\upsilon\pi 2(2)$ at a fixed toroidal field, relaxing the existing constraints imposed by the plasma stability even by a modest amount can lead to a significant increase in fusion power production. In this regard, an extensive body of research has been, and continues to be conducted to better understand and characterize the stability limits of tokamak plasmas [20]. In addition to observing and diagnosing specific plasma instabilities, an understanding of how instability thresholds scale with plasma parameters is important for determining optimal methods of machine operation to maximize fusion power production.

The scaling of the beta limit due to disruptions at high plasma stored energy has been examined to help quantify the level of fusion power and $Q_{sdo2(DT)}$ that may be attained in TFTR. Combining the scalings of fusion power or $Q_{sdo2(DT)}$, $\beta_{sdo2(N)}$ (which is derived from the scaling of stored energy) and the beta limit, the optimal operating value of $H_{sdo2(ne)}$ producing maximum fusion power or Q_{DT} can be derived for a discharge of given parameters.

It has been demonstrated that the improved energy confinement and neutron production of beam heated discharges in TFTR is largely independent of the plasma parameters such as plasma current, edge safety factor, and toroidal field up to the time of the peak of stored energy. However, these parameters are important in the determination of the stability limits of plasma operation. For example, the upper limit of the performance of non-disrupted discharges is a strong function of magnetic field as shown in Fig. 8. Here, the central beam fueling (Psdo2(B)Hsdo2(ne)) is used as a figure of merit for discharges that increased in performance as the toroidal field was increased. Note that plasmas with RS magnetic configuration has achieved higher Psdo2(B)Hsdo2(ne) for the same toroidal field compared to other plasmas.

As shown in Fig. 9, the conventional Troyon β-limit [21], $\beta\sigma\delta o2(N) \sim 2.4$ provides a good characterization of the disruptive beta limit for TFTR plasmas in which no particular equilibrium profile modification has been employed. The shaded areas represent the operating range of non-disrupted discharges at different major radius. However, it has been demonstrated that variations of both the current and pressure profile shapes can lead to substantial changes to the maximum acheivable $\beta_{sdo2(N)}$ in TFTR [7, 22, 23] and other devices including DIII-D [24]. Therefore, while a considerable number of plasmas in TFTR terminate in disruption at $\beta_{sdo2(N)} \sim 2.4$, many plasmas are observed to disrupt at considerably lower values of $\beta_{sdo2(N)}$ as shown in Fig. 9. For example, in plasmas with intensive lithium wall conditioning [10], it has been demonstrated that the best performance discharges disrupted at $\beta\sigma\delta o2(N) < 2$. It was found that Psdo2(B)Hsdo2(ne) (the central beam fueling or deposition) reached a value of about 95 for DD discharges and 75 for DT discharges, respectively. The disrupted discharges at $\beta sdo2(N) < 2$ had extremely high Hsdo2(ne) (up to 6.2) which suggests that the pressure profile is extremely peaked. This suggestion has been verified by equilibrium and transport analyses of the relevant plasmas. On the other hand, plasmas with reduced pressure peakedness and increased current profile peakedness have yielded $\beta_{sdo2(N)}$ as large as 4.9 in TFTR [25]. These results are consistent with the ideal MHD stability modeling of these plasmas which shows that an increase of the plasma internal inductance, $l_{sdo2(i)}$ (a peaking of the current profile) can lead to an increase in the maximum stable

$\beta_{sdo2(N)}$ value, while an increase in pressure profile peakedness generally leads to a reduction in the maximum $\beta_{sdo2(N)}$ value [23].

In assessing the dependence of the disruptive $\beta_{\sigma\delta o2(N)}$ limit on equilibrium profile variations, TFTR plasmas from each confinement regime including L-mode, Supershot, high poloidal beta, reversed shear, and enhanced Supershot using lithium wall conditioning, have been considered. The maximum $\beta_{\sigma\delta o2(N)}$ due to disruptions in TFTR plasmas is plotted in Fig. 10. For plasmas with $H_{ne} > 2.3$, a linear fit to the data shown in Fig. 10 yields

$$\beta_{N\,max} = 4.12\ \mathrm{f}(F_{I_p}, H_{ne}) + 0.5\ . \qquad [8]$$

Here, the more convenient experimental parameters F_{I_p} (plasma current ramp factor) and $H_{sdo2(ne)}$ have been used as independent variables, rather than l_i and pressure peakedness factor. The factor F_{I_p} is used to simulate the variation in $\beta_{sdo2(N)}$ observed with varying l_i in plasmas which utilize current ramping techniques to alter the current profile. This factor, which increases linearly with increasing l_i, is defined as the ratio of the plasma current before the current ramp to that after the current ramp (a discharge with constant Isdo2(p) has $F_{I_p} = 1$). For these plasmas in TFTR, the equation $l_i = 1.25\ F_{I_p}$ can be used as a conversion between these two variables. The variable $H_{sdo2(ne)}$ is used here to model the reduction of $\beta_{sdo2(N)}$ observed at increased values of pressure profile peaking.

It is important to realize that Eq. [8] is best used as a simple guide to the behavior of the stability limit when current and pressure profile modifications are introduced sufficiently similar to the plasmas used to create the relation. For example, one case not covered sufficiently by the original dataset is that of plasma disruptions at low values of $H_{sdo2(ne)} < 2$. Since these plasmas typically have poor (L-mode) confinement in TFTR, the disruptive beta limit has not been systematically tested in these plasmas. Therefore, it is presently not clear that an increase in the maximum $\beta_{sdo2(N)}$ can be reached by reducing $H_{sdo2(ne)} < 2$ in TFTR. Analysis of more complete and accurate models of the disruptive beta limit at high l_i and pressure profile peakedness in TFTR is presently underway.

Based on this uncertainty, a conservative interpretation of Eq. [8] is that the standard Troyon coefficient is increased by increasing the current profile peakedness, but can only be decreased by increasing the pressure peakedness (modeled here by H_{ne}^{-1}). Physically, this latter reduction in the stability limit at $H_{ne} > 2.3$ is interpreted as being due to a central, rather than a global beta limit. At lower values of H_{ne}, the plasma would then return to a global, rather than a local beta limit. This prescription leads to a more restrictive beta limit which is consistent with the existing data.

5. OPERATIONAL PERFORMANCE DIAGRAM

By combining the scalings for fusion reactivity, plasma stored energy, and the disruptive beta limit, a useful operational "roadmap" to tokamak performance can be created. For TFTR, using the derived scaling for the total stored energy (Eq. 6), and eliminating stored energy in favor of $\beta_{\sigma\delta o2(N)}$ by

$$\text{i} \qquad (,,p\ dv) = f(p\ \beta_N\ R\ \kappa\ I_p\ a\ B_0, 40) \qquad [9]$$

an operational diagram including both bsdo2(N) and fusion power (or Q) contours in the space ($H_{sdo2(ne)}$, $P_{sdo2(B)}$) can be made once the parameters R, a, I_p, κ, and B_0 are specified. For DT plasmas, a multiplicative constant of 1.2 is used to model the increase in stored energy observed due to the "isotope effect". The diagram containing this information is useful in both a predictive and interpretive fashion.

As an example, the operational performance diagram for I_p = 1.2 MA high $\beta_{sdo2(N)}$ plasmas created during the DT phase of TFTR is shown in Fig. 11. This data nicely summarizes the operational domain in $H_{sdo2(ne)}$ and $P_{sdo2(B)}$ covered by the experiment. The majority of the plasmas shown are deuterium plasmas, which are indicated by open circles, while DT plasmas are indicated by filled squares. Note that in this particular figure, the contours of $\beta_{sdo2(N)}$ are relevant for the D plasmas. As

shown, the D plasma data predicts what values of $\beta_{sdo2(N)}$ would be obtained if D only, rather than DT were to be used. The bold contours shown predict the values of fusion power, P_f, that would be reached if DT fuel were used. Note that since equations [5] and [6] are based on plasmas which generally last several energy confinement times, these contours generally do not accurately predict the performance of disruptions.

As discussed in the previous section, the beta limit shown in Fig. 11 for $H_{sdo2(ne)} < 2.3$ is chosen to follow a contour of constant $\beta_{sdo2(N)}$, while this limit is reduced (as modeled by equation [8]) for $H_{sdo2(ne)} > 2.3$. This suggests for a given set of plasma parameters that an optimum point for Psdo2(f) exists in the space ($H_{sdo2(ne)}$, $P_{sdo2(B)}$) at an intermediate level of $P_{sdo2(B)}$. The results show that the stable operating space computed for these parameters was well covered by the experiment, and that three plasmas with excessively large values of $H_{sdo2(ne)}$ terminated in disruption. Two plasmas, one at, and one just above the modeled $\beta_{sdo2(N)max}$ contour did not disrupt. A deuterium plasma was generated with $P_{sdo2(B)} = 25.5$ MW and $H_{sdo2(ne)} = 2.1$, which is predicted to have produced greater than 5 MW of fusion power had an equivalent DT shot been taken. This point lies near the optimal operating point yielding $P_{sdo2(f)} = 6$ MW for this condition. The maximum $P_{sdo2(f)}$ actually produced in a DT plasma in these conditions is shown to be 4.2 MW.

The operational performance diagram for a subset of TFTR Supershots that have reached the maximum P_f and Q_{DT} is shown in Fig. 12. Two contours of $\beta_{N\,max}$ are shown to describe two datasets with different plasma current - one with $I_p = 2.3$ MA for $P_{sdo2(B)} < 23$ MW and one with $I_p = 2.7$ MA for $P_{sdo2(B)} > 23$ MW. It is interesting to note that the discharge with the highest fusion power (Psdo2(B) ~ 40 MW) has a similar Qsdo2(DT) compared to the discharge with high Hsdo2(ne) at moderate Psdo2(B) ~ 17 MW.

Based on this data, it is instructive to map out how one could proceed to reach $Q_{DT} > 1$. The data shown in Fig. 12 demonstrates that high values of Qsdo2(DT) can be reached at reduced Psdo2(B) and increased Hsdo2(ne). As also clearly shown by the Q and $\beta_{\sigma\delta o2(N)}$ contours, this scenario would

clearly lead to maximized Qsdo2(DT) if it were not for the reduction in $\beta_{sdo2(N)max}$ at high Hsdo2(ne). Fig. 12 shows that once we consider Eq. 8 for the stability limit at sufficiently large Hsdo2(ne), the gain in Qsdo2(DT) is negated at reduced Psdo2(B) and increased Hsdo2(ne). Moving to a larger Qsdo2(DT) requires that $\beta_{sdo2(N)max}$ be pushed to greater values of Qsdo2(DT). By equating the relevant physics parameter l_i for F_{Ip} in Eq. 8, we find that this can be accomplished by an increase in the product $(B_T\, l_i\, I_p)$ / Hsdo2(ne), while maintaining high τ_E through increased Hsdo2(ne). Considering that the unfavorable inverse dependence of $\beta_{sdo2(N)max}$ on Hsdo2(ne) is applicable in the range Psdo2(B) ≥ 25 MW, an example solution which gives a $\beta_{sdo2(N)max}$ contour at Qsdo2(DT) = 1 (see Fig. 12) would be B_T = 7.6 T, I_p = 3.8 MA, and a doubling of l_i. Such large increases in l_i have been produced transiently in tokamaks including TFTR [7] and DIII-D [26, 27]. Certainly, solutions other than increasing l_i exist to produce the increased stability required to allow access to Qsdo2(DT) = 1. Plasma shaping has long been consider one such approach, as well as reversing the central shear of the *q* profile [8,28], which is presently being explored in TFTR and DIII-D.

Regardless of the technique used to increase stability, a corresponding increase in τ_E is also required to avoid excessive levels of P_B at Qsdo2(DT) = 1. Eq. 7 indicates that reaching scientific breakeven would require a value of the product P_BHsdo2(ne) ~ 200, which is more than double the largest value reached to date (Fig. 9). Due to increased wall particle fueling and the consequent neutral beam attenuation, reaching increased levels of Hsdo2(ne) (corresponding to increased τ_E) becomes more difficult at increased P_B, however, this constraint has been somewhat relaxed by recent limiter conditioning techniques [10]. Constraints on Hsdo2(ne) due to beam attenuation of "marginal" NBI sources are of equal importance to plasma stability issues. These constraints may fortunately be relieved by improved neutral beam technology. For example, high energy negative-ion neutral beam sources, which are presently being installed to deliver high power to the JT-60U tokamak [29] may provide sufficiently peaked beam deposition profiles in high density plasmas. In the range of 40 MW input power, Fig. 12 shows that a factor of approximately 2.5 improvement in Hsdo2(ne) would be required to reach Qsdo2(DT) = 1 over present data. This result emphasizes the importance of neutral beam technology development if such heating sources are to be used to increase Hsdo2(ne) in high Q

tokamak devices.

6. PHYSICS OF NEUTRAL BEAM HEATED PLASMAS IN OTHER TOKAMAKS

It is also striking to find that the effect of Hsdo2(ne) on the performance of beam heated discharges discussed for TFTR are not unique. A similar interpretation of energy confinement and fusion reactivity can be found in other tokamaks where the profile characteristics and edge conditions (limiter vs. divertor) are vastly different. Even though, the neutral beam heating sources used in most tokamaks are more or less similar to the beam sources employed in TFTR, there are significant differences in the beam fueling profile due to the beam line arrangement and operating plasma positions. In addition to the differences in engineering configuration, the time evolution of plasma density profiles can influence the dependence of the performance on Hsdo2(ne).

The TEXTOR tokamak reported "I-mode" regime [30] in which the energy confinement time of the beam heated discharges was improved by up to a factor of two compared to ITER-89P scaling. TEXTOR is very similar to the TFTR in many respects except size; circular plasma with a limiter. The TEXTOR had a tangential system simlar to TFTR with a beam energy of ~ 50 keV and a recent study based on TRANSP analysis [13] showed that Hsdo2(ne) $\propto$ Fsdo2(0.5,ne) EXP(-0.3nsdo2(e)) which is slightly different from TFTR expression (Eq. 2). When Hsdo2(ne) was included in the scaling study, a factor of two variation of energy confinement time was easily explained [31].

It has been known that shaped plasmas (discharges with divertor) have differences from circular plasmas, since the profiles appear to be broader and stability limits larger. Due to a relatively small contact point with the wall (X-point in the divertor), there is a distinctive advantage in the particle influx control. However, it is quite a surprise to find that there are similarities in the performance improvement in a diverted plasma. For instance, the fusion power gain for the beam heated discharges in JET is shown to be "Qsdo2(DD $\propto$ Psdo2(B))(central)" [32] which can be a qualitative interpretation of the derived result for TFTR (Eq. [7]). From this result, it is not difficult to deduce that improved

energy confinement is connected through the relationship studied in this paper. The NBI systems on the JET tokamak are equipped with two different beam energies (~140 keV and ~80 keV) and allowed on-axis tangential injection. However, recent modifications implemented for a divertor study have led to an off-axis tangential heating system due to the imposed upward shift of the plasma position. This may not be entirely responsible for the observed degraded performance following the installation of new divertor system but it provides a logical interpretation of the result [33]. The fact that the plasmas with an increased elongation on JET did not improve the performance [34] whereas a similar experiment in DIII-D yielded improved performance [34] is an intriguing problem. One must note that the increased elongation in JET plasmas implies that the central beam fueling is further degraded, however the result is opposite on DIII-D. The DIII-D tokamak has a tangential injection system with a beam energy of approximately 90 keV. Furthermore, the recent high performance result [35] from DIII-D reminds us that the peakedness of the beam fueling (90 % central beam fueling) is primarily responsible for the enhanced fusion reactivity.

The JT-60U tokamak is equipped with a flexible but mainly off-axis heating system for a full size plasma (Vsdo2(p) = 60 msup2(3)) operation with a beam energy of approximately ~90 keV. On JT-60U, the discharges with the best performance have been created in the high poloidal beta, βsdo2(p), regime obtained when a relatively small plasma (Vsdo2(p) = 37 msup2(3)) was formed toward the high field side of the vacuum vessel which allows central beam fueling [36]. Note that the beam deposition is always hollow for a full size plasma on JT-60U. Although a successful initial attempt was made to unify results [37] between TFTR Supershot and JT-60U high βsdo2(p) regimes based on beam fueling profile shape, lack of reliable density information in the JT-60U high βsdo2(p) regime and possible intrinsic differences between divertor and limiter plasmas requires more careful study.

As far as beam heated plasmas in tokamaks are concerned, plasma performance can be explained by the scalings based on the beam fueling profile. It is important to understand and incorporate the differences in stability limits between limiter and divertor discharges in order to implement a study similar to the TFTR results.

6. SUMMARY

Scalings of the ion and electron energy, neutron yield, and stability limits have been derived for TFTR beam heated plasmas which include L-mode, Supershot, high bsdo2(p), and reversed shear confinement regimes in TFTR. The ion stored energy is linearly correlated with the central beam fueling. It has been shown that the ion stored energy is insensitive to the plasma current and edge safety factor and toroidal field. The electron stored energy is found to be insensitive to Hsdo2(ne) and the dependence on plasma current is relatively strong. The deduced absolute scalings for the global stored energy and fusion reactivity are applied to D discharges at different major radius with various wall conditions, and DT discharges at various regimes such as L-mode, Supershots, and high βsdo2(p). Even though the performance of the discharges are insensitive to the plasma current and toroidal field, these plasma parameters are extremely important in the determination of the disruptive stability boundary of beam heated discharges. Based on the study result, it is conceivable to project a tokamak with Q>1 with present technology. In addition, it is pointed out that the performance characteristics of TFTR beam heated discharges are not unique. Similar physics interpretation can be applied to the results obtained in other devices such as JET, D-IIID, TEXTOR, and JT-60U, which can have vastly different plasma profile shapes.

ACKNOWLEDGMENT

This work was supported by U.S. DoE contract No. DE-ACO2-76-CHO-3073 and DE-FG02-89ER53297. Thanks go to S. D. Scott for the Figure 1.

Figure Captions

Figure 1. The global energy confinement time (τσδo2(E)) measured at the time of maximum stored

energy is shown as a function of a various edge parameters such as Csup2(+2) emission (a), Hsdo2(α) emission (b), edge electron density (c) and beam fueling parameter (Hsdo2(ne)) (d) for discharges with a fixed major radius. The correlation between τσδo2(E) and Hsdo2(ne) is shown to be excellent. A few data points marked such as 244 (shot # 68244) and 242 (shot # 68242) which do not quite fit with the edge parameters are well correlated Hsdo2(ne).

Figure 2. The influence of Hsdo2(ne) on the ion stored energy is demonstrated for beam heated discharges. The ion stored energy is nearly a linear function of the central beam fueling parameter (Psdo2(1.3,B)Hsdo2(0.8,ne)).

Figure 3. The measured DD fusion neutron emission (Ssdo2(n)) is compared to the scaling CWsdo2(1.6,i). Deviation from square can be attributed to the beam target reaction in addition to the thermo-nuclear reaction.

Figure 4. The ratio of the measured Wsdo2(tot) and estimated Wsdo2(P,tot) is illustrated as a function of edge safty factor (*qsdo2(a)*). Note that Wsdo2(,P,tot) does not have a explicit dependence on the edge safety factor (*qsdo2(a)*)

Figure 5. Comparison of the measured and modeled Wsdo2(tot) and Ssdo2(n) in D plasmas. (a) In order to demonstrate that the major radius does not dependent upon the stored energy, the measured stored energy is depicted as a function of Wsdo2(p,tot) for discharges obtained at three different major radius. (b) Discharges with RS magnetic configuration obtained at Rsdo2(o) = 2.62 m are compared with Wsdo2(p,tot) together with L-mode discharges and Supershots at Rsdo2(o) = 2.52 m.

Figure 6. (a) The measured stored energy of DT discharges (supershots and L-mode discharges) with a mixture ranging from 30 % to 70 % is compared with 1.25 x Wsdo2(p,tot). Multiplieer 1.25 is attributed to the “isotopic effect” from the usage of Tritium. (b) The neutron yield from DT discharges is compared to 72 x Ssdo2(p,n) . The neutron scalar from D to DT plasma can be 144.

Figure 7. The ratio of the measured global stored energy to that derived scaling (Wsdo2(p,tot)) for D and DT discharges with various toroidal field is shown. Note that Wsdo2(p,tot) does not have explicit dependence on Bsdo2(T). For DT discharges, the multiplier was accounted.

Figure 8. The central beam fueling (Psdo2(B)Hsdo2(ne)) for non-disrupted discharges is depicted as a function of toroidal field. Discharges with RS magnetic configuration extend further than other beam heated discharges.

Figure 9. The operational range of beam heated discharges on TFTR is shown in a space spanned by βsdo2(N) and the central beam fueling parameter (Psdo2(B)Hsdo2(ne)). The shaded areas are representing operating ranges without disruptions. As performance is increased, discharges are disrupted at an extremely low normalized beta. It appears that DT discharges are disrupting at Psdo2(B)Hsdo2(ne) ~75 and D discharges are disrupting at Psdo2(B)Hsdo2(ne) ~ 95. The difference can be ~ 25 % which is consistent with "isotopic effect".

Figure 10. The maximum β_N attained in TFTR beam heated plasmas prior to disruption. The linear fit to the data shown is used to characterize the changes in the β_N limit due to variations in current and pressure profile modification, modeled here using the parameters F_{Ip} (plasma current ramp factor) and $H_{sdo2(ne)}$.

Figure 11. Operational performance diagram for high β_p plasmas with I_p = 1.2 MA and F_{Ip} = 1.49. Open symbols represent D-only plasmas, while solid symbols represent DT plasmas. Bold, solid lines represent contours of P_f, while thin, dashed lines are contours of β_N. The heavy dashed contour is the stability limit as given by equation [8] for Hsdo2(ne) > 2.3 and β_N = 3.2 for Hsdo2(ne) < 2.3 .

Figure 12. Operational performance diagram for TFTR Supershot plasmas which have reached the maximum fusion power and Q_{DT} to date. Two datasets are shown, one with I_p = 2.3 MA for $P_{sdo2(B)}$ < 23 MW and the other with I_p = 2.7 MA for $P_{sdo2(B)}$ > 23 MW. Bold, solid lines represent contours of Q_{DT}, while thin, solid lines are contours of β_N. The heavy dashed contour is the stability limit as given by equation [8] for the dataset with I_p = 2.7 MA.

†Present address: Princeton Plasma Physics Laboratory, Princeton University, Princeton, N.J. 08543

[1] Strachan, J., M. Bitter, Ramsey, A.T., Zarnstorff, M.C., *et al.,* Phys. Rev. Lett. **58**, (1987), 1004

[2] Strachan, J., Nucl. Fusion, **34** (1994), 1017

[3] Park, H.K., Bell, M.G., Tang W., *et al.*, Nucl. Fusion **34** (1994), 1217

[4] Park, H.K., Barnes, C.W., Budny, R., *et al.*, Nucl. Fusion **32** (1992), 1042.

[5] Goldston R.J., Plasma Phys., **26** (1984), 87.

[6] Rebut, P.H., Lallia, P.P., Watkins, M.L., in Plasma Physics and Controlled Nuclear Fusion Research 1988 (Pro. 12th Int. Conf. Nice, 1988), Vol.2, IAEA, Vienna (1989) 191.

[7] Sabbagh, S.A., Gross, R.A., Mauel, M.E.., *et al*.., Phys. Fluids B **3** (8), (1991), 2277.

[8] Levinton, F., Zarnstorff, M.C., Batha, S.H., *et al.,* Phys. Rev. Lett. **75**, (1995), 4417

[9] Mansfield, D.K., Strachan, J.D., Bell, M.G., *et al.*, to be published in Physics of Plasmas.

[10] Mansfield, D.K., *et al.,* to be published in Physics of Plasmas.

[11] S. Scott, M. C. Zarnstorff, C. W. Barnes, *et al.*, *Phys. Plasmas* **2** (1995) 2299.

[12] Chang, Z, Fredrickson, E.D., Callen, J.D., *et al.,* Nucl. Fusion 34, 1309 (1994)

[13] Budny, R.V., Nucl. Fusion, **34**, (1994), 1205.

[14] Hulse, R.A., Cavallo, A., Johnson, D., *et al.*, Proc. 17th EPS Conf. on Controlled Fusion and Plasma Physics, Amsterdam, The Netherlands, 1990 (European Physical Society, Amsterdam, 1990) 174.

[15] Batha, S., Levinton, F., Scott, S.D., *et al.*, to be published in Physics of Plasmas, 1996

[16] Park, H.K., Goldston, R.J., G. Taylor, in Proceedings of the 4th international Symposium on Laser-Aided Plasma Diagnostics, (Fukuoka, Japan, Nov. 1989), 17-25.

[17] Zarnstorff, M., Bateman, G., Batha, S., *et al.*, Paper IAEA-CN-56/A-2-2 presented at the 14th Internation Conference on Plasma Physics and Controlled Nuclear Fusion Research (Wurzburg, Germany, 1992).

[18] Strachan, J.D., Adler, H., Alling, P., *et al.*, Phys. Rev. Lett., **72**, (1994), 3526.

[19] Hawryluk, R.J., Adler, H., Alling, P., *et al.*, Phys. Rev. Lett., **72**, (1994), 3530

[20] Taylor, T., *Proceedings of the Varenna Workshop on Tokamak Concept Improvement*, (S. Bernabei,

N. Sauthoff, E. Sindoni, eds.) Varenna, Italy, 1994, Editrice Compositori, Bologna, p. 111, and references therein.

[21] Troyon, F., Gruber, R., *et al.*, Plasma Phys. Controlled Fusion **30**, (1988), 209.

[22] Mauel, M.E., Navratil, G.A., Sabbagh, S.A., *et al.*, in *Proceedings of the Fourteenth International Conference on Plasma Physics and Controlled Nuclear Fusion Research*, (Wurzburg, Germany, September 1992) (International Atomic Energy Agency, Vienna, Austria, 1993) Vol. 1, p. 205.

[23] Mueller, D., *et al.*, "Disruption Avoidance in TFTR", to be published in Fusion Technology.

[24] Howl, W., Turnbull, A., Taylor, T., *et al.,* Phys. Fluids B **4** (1992) 1724.

[25] Sabbagh, S.A., Mauel, M.E., Navratil, G.A., *et al.,* in Proceedings of the Fifteenth International Conference on Plasma Physics and Controlled Nuclear Fusion Research, (Seville, Spain, September 1994) (International Atomic Energy Agency, Vienna, Austria, 1995) Vol. 1, p. 663.

[26] Ferron, J.R., *et al.*, Phys. Fluids B **5** (1993) 2532.

[27] Lao, L.L., *et al.,* Phys. Rev. Lett. **70** (1993) 3435.

[28] Sabbagh, S.A., Hughes, M.W., Phillips, M.W., *et al.*, Nuclear Fusion, **29** (1989) 423.

[29] JT-60 Team, in Proceedings of the Fifteenth International Conference on Plasma Physics and Controlled Nuclear Fusion Research, (Seville, Spain, September/October 1994), (International Atomic Energy Agency, Vienna, Austria) Vol. I, 211, Paper IAEA-CN-60/A2-4

[30] Ongena J., Conrads., H., Gaigneaus, M., *et al.*, Nucl. Fusion, **33**, (1993), 283.

[31] Park, H.K., Budny, R.V., Ongena, J., *et al.*, to be submitted to Nucl. Fusion.

[32] Thompson, E., Stork, D., de Esch, H.P.L., and the JET Team, Phys. Fluids B 5 (7), (1993), 2468

[33] JET Team, in Proceedings of the Fifteenth International Conferenceon Plasma Physics and Controlled Nuclear Fusion Research, (Seville, Spain, September/October 1994), (International Atomic Energy Agency, Vienna, Austria) Vol. I, 211, Paper IAEA-CN-60/A2-4

[34] Greenfield, C.M., DeBoo, J.C., Osborne, T.H., et al., Bull. of APS, 36th Annual meeting of the Division of Plasma Physics, paper 5P2, (1994) 1644

[35] Rice, B.C., Bull. of APS, 37th Annual meeting of the Division of Plasma Physics, 1995, to be published in Phys, of Plasma.

[36] JT-60U Team, in Proceedings of the Fifteenth International Conferenceon Plasma Physics and

Controlled Nuclear Fusion Research, (Seville, Spain, September/October 1994), (International Atomic Energy Agency, Vienna, Austria) Vol. I, 31, Paper IAEA-CN-60/A1-2

[37] Park, H.K., Bell, M., Ishida, S., in Proceedings of the Fifteenth International Conference on Plasma Physics and Controlled Nuclear Fusion Research, (Seville, Spain, September/October 1994), (International Atomic Energy Agency, Vienna, Austria) Vol. II, 211, Paper IAEA-CN-60/4-p-1

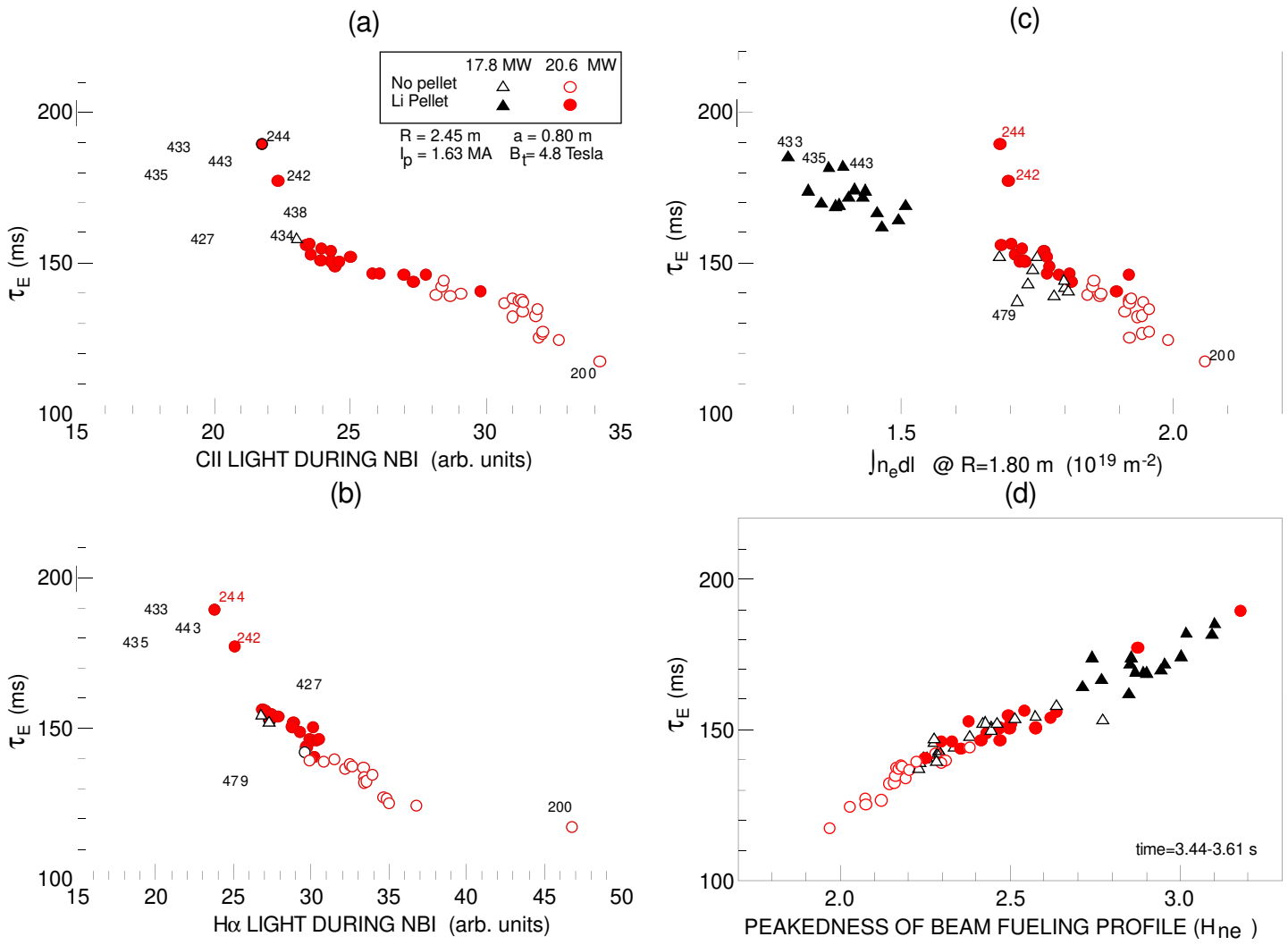
(a)
17.8 MW 20.6 MW
No pellet
Li Pellet
R = 2.45 m a = 0.80 m
I_p = 1.63 MA B_t= 4.8 Tesla
τ_E (ms)
CII LIGHT DURING NBI (arb. units)
(b)
Hα LIGHT DURING NBI (arb. units)
(c)
$\int n_e dl$ @ R=1.80 m (10^{19} m^{-2})
(d)
PEAKEDNESS OF BEAM FUELING PROFILE (H_{ne})
time=3.44-3.61 s

Fig. 1

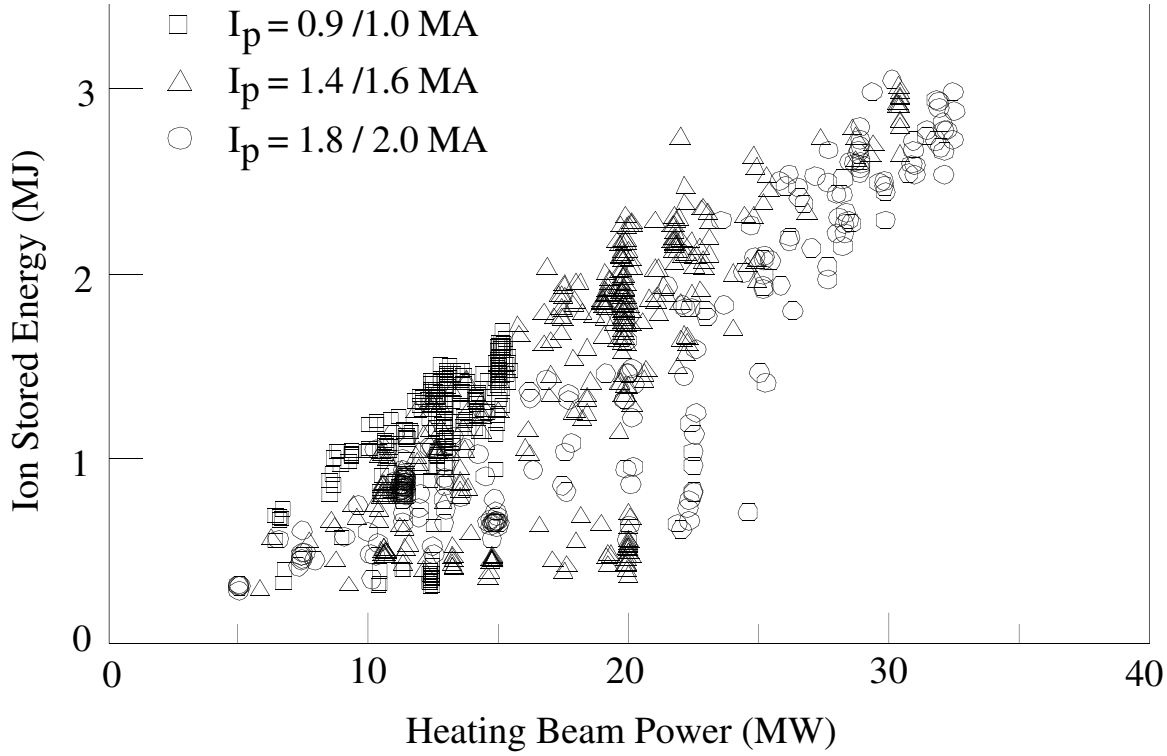
I_p = 0.9 /1.0 MA
I_p = 1.4 /1.6 MA
I_p = 1.8 / 2.0 MA
Ion Stored Energy (MJ)
Heating Beam Power (MW)
0
1
2
3
0
10
20
30
40

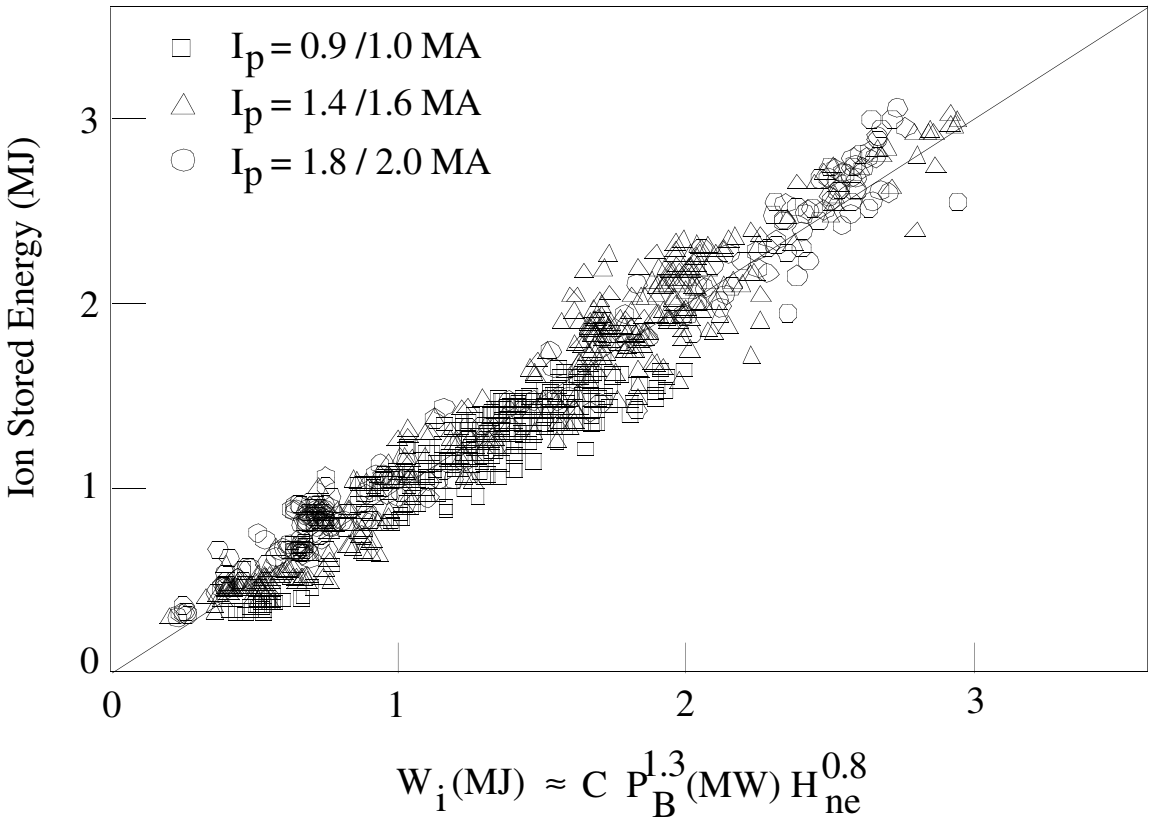
I_p = 0.9 /1.0 MA
I_p = 1.4 /1.6 MA
I_p = 1.8 / 2.0 MA
Ion Stored Energy (MJ)
$W_i(MJ) \approx C\ P_B^{1.3}(MW)\ H_{ne}^{0.8}$
0
1
2
3

Fig. 2

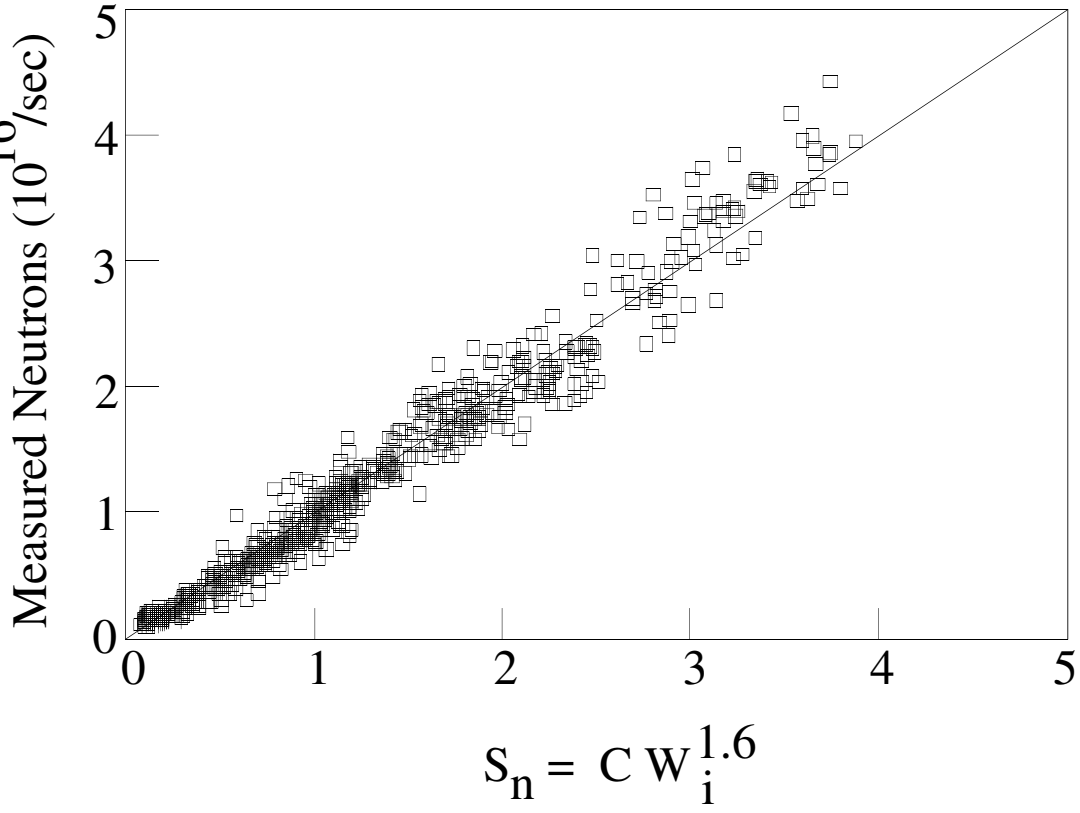
Measured Neutrons (10^{16}/sec)
0
1
2
3
4
5
$S_n = C W_i^{1.6}$

Fig. 3

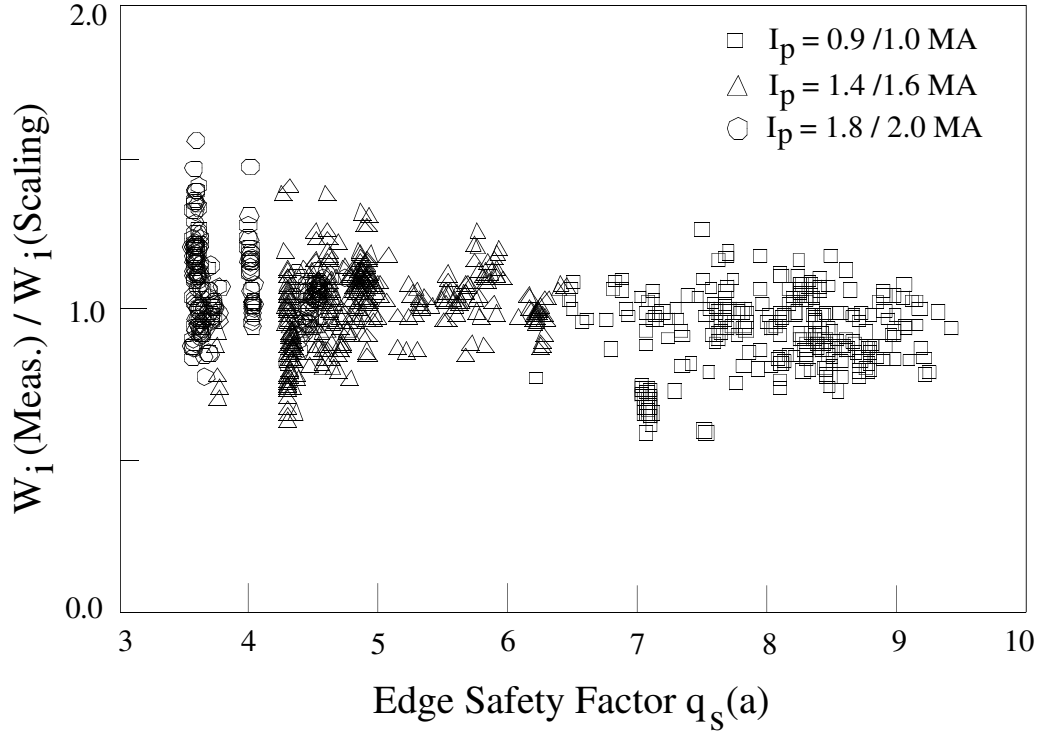
I_p = 0.9 /1.0 MA
I_p = 1.4 /1.6 MA
I_p = 1.8 / 2.0 MA
W_i (Meas.) / W_i (Scaling)
0.0
1.0
2.0
3
4
5
6
7
8
9
10
Edge Safety Factor $q_s(a)$

Fig. 4

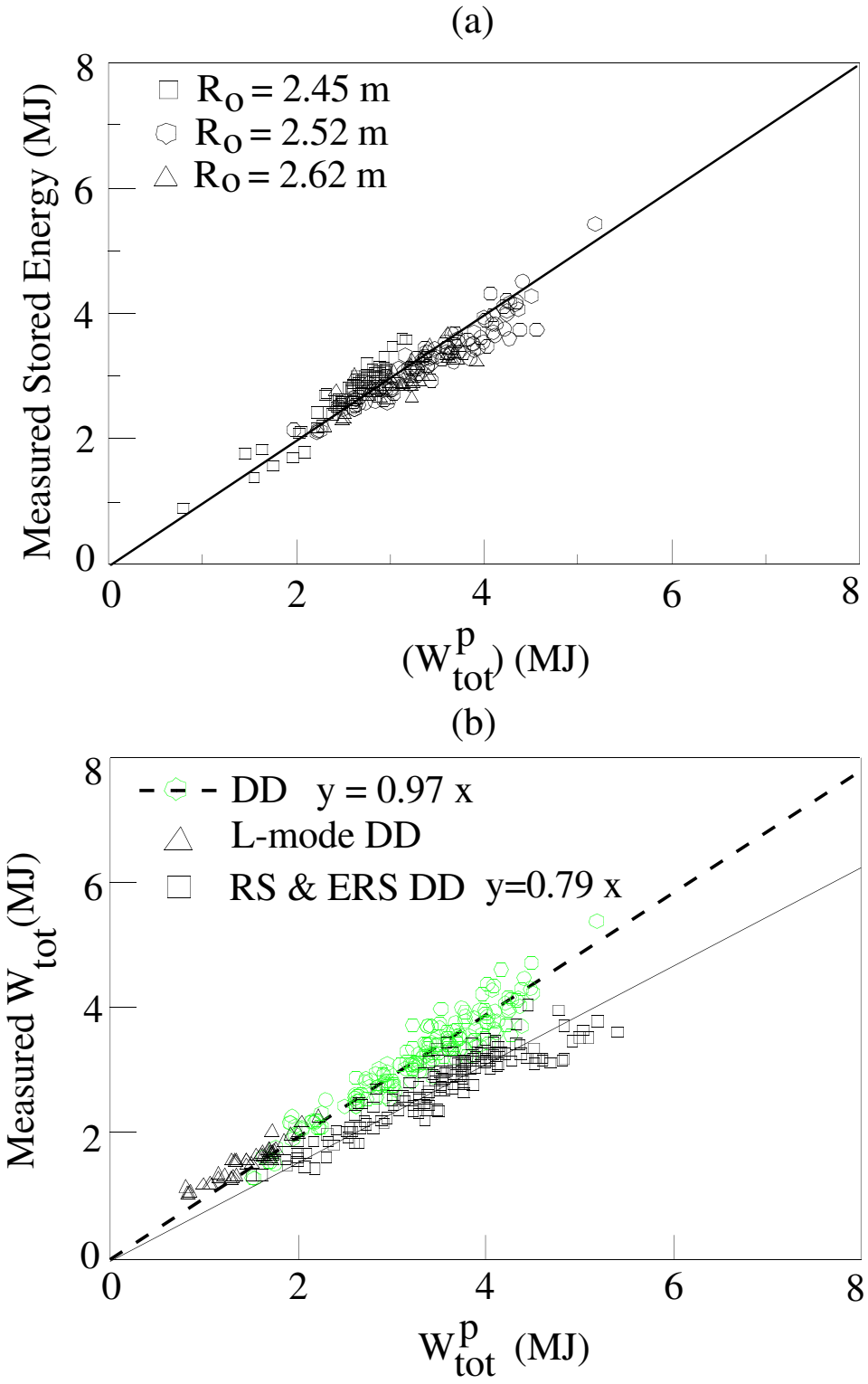
(a)
Measured Stored Energy (MJ)
R_o = 2.45 m
R_o = 2.52 m
R_o = 2.62 m
(W_{tot}^{p}) (MJ)
(b)
Measured W_{tot}(MJ)
DD y = 0.97 x
L-mode DD
RS & ERS DD y=0.79 x
W_{tot}^{p} (MJ)

Fig. 5

(a)

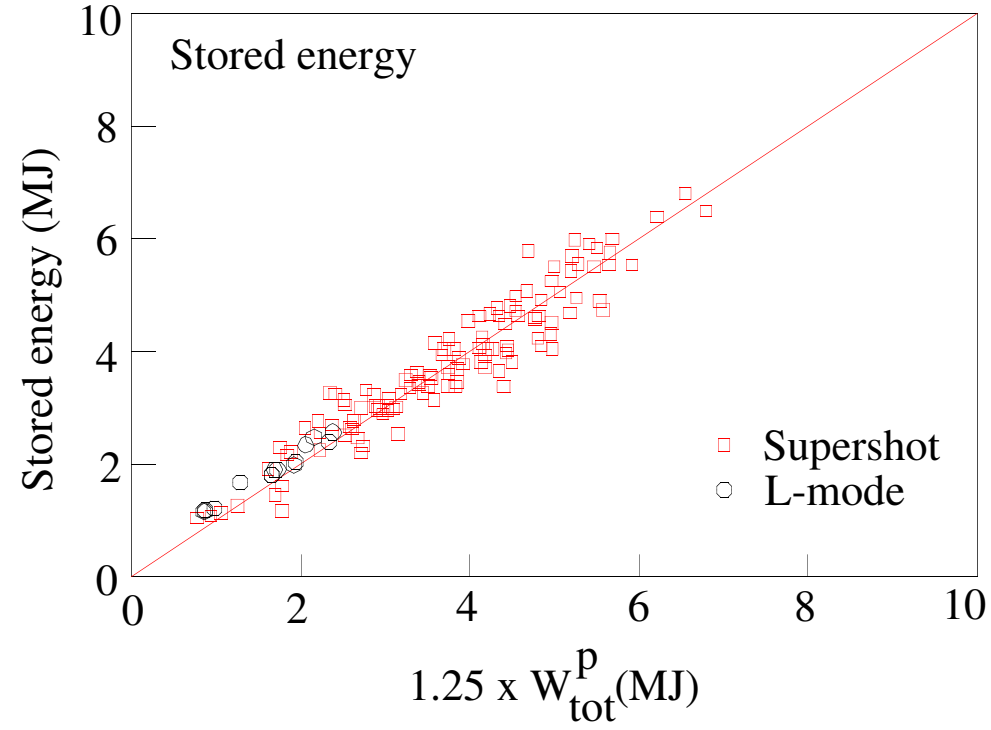
Stored energy
Stored energy (MJ)
1.25 x W^{p}_{tot}(MJ)
Supershot
L-mode
0
2
4
6
8
10

(b)

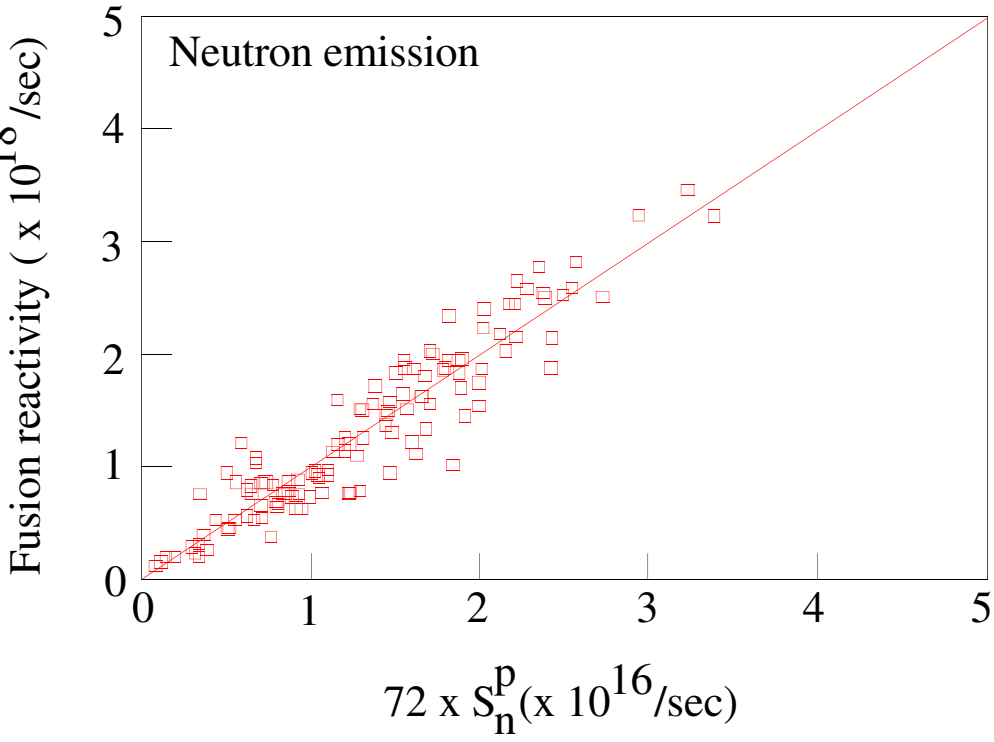
Neutron emission
Fusion reactivity (x 10^{18}/sec)
72 x S^{p}_{n}(x 10^{16}/sec)
0
1
2
3
4
5

Fig 6

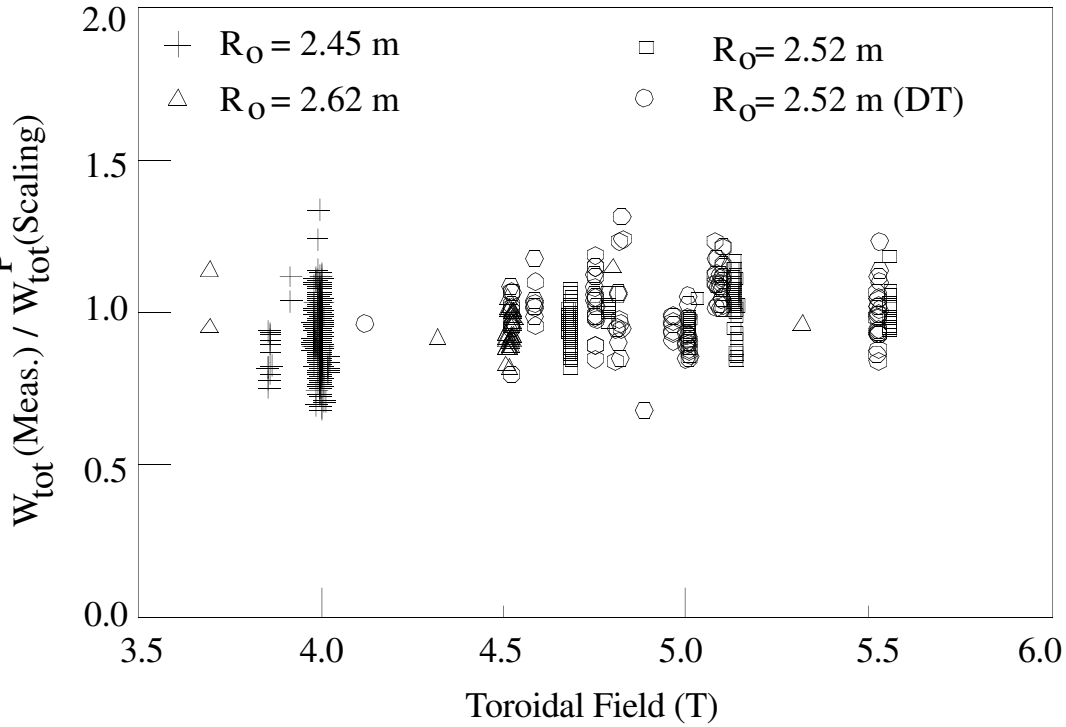
2.0
1.5
1.0
0.5
0.0
3.5
4.0
4.5
5.0
5.5
6.0
R_o = 2.45 m
R_o = 2.62 m
R_o= 2.52 m
R_o= 2.52 m (DT)
W_{tot}^{P} (Meas.) / W_{tot}(Scaling)
Toroidal Field (T)

Fig. 7

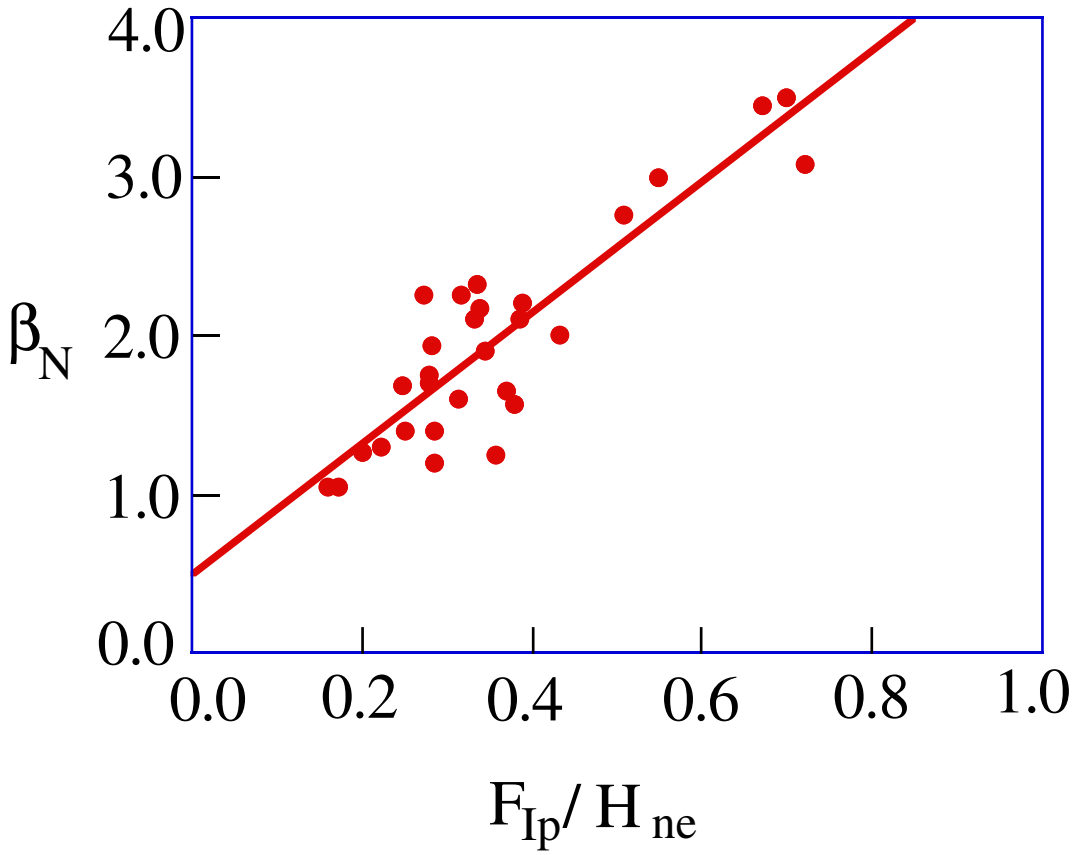
4.0
3.0
2.0
1.0
0.0
0.0
0.2
0.4
0.6
0.8
1.0
β_N
F_{Ip}/ H_{ne}

Fig. 8

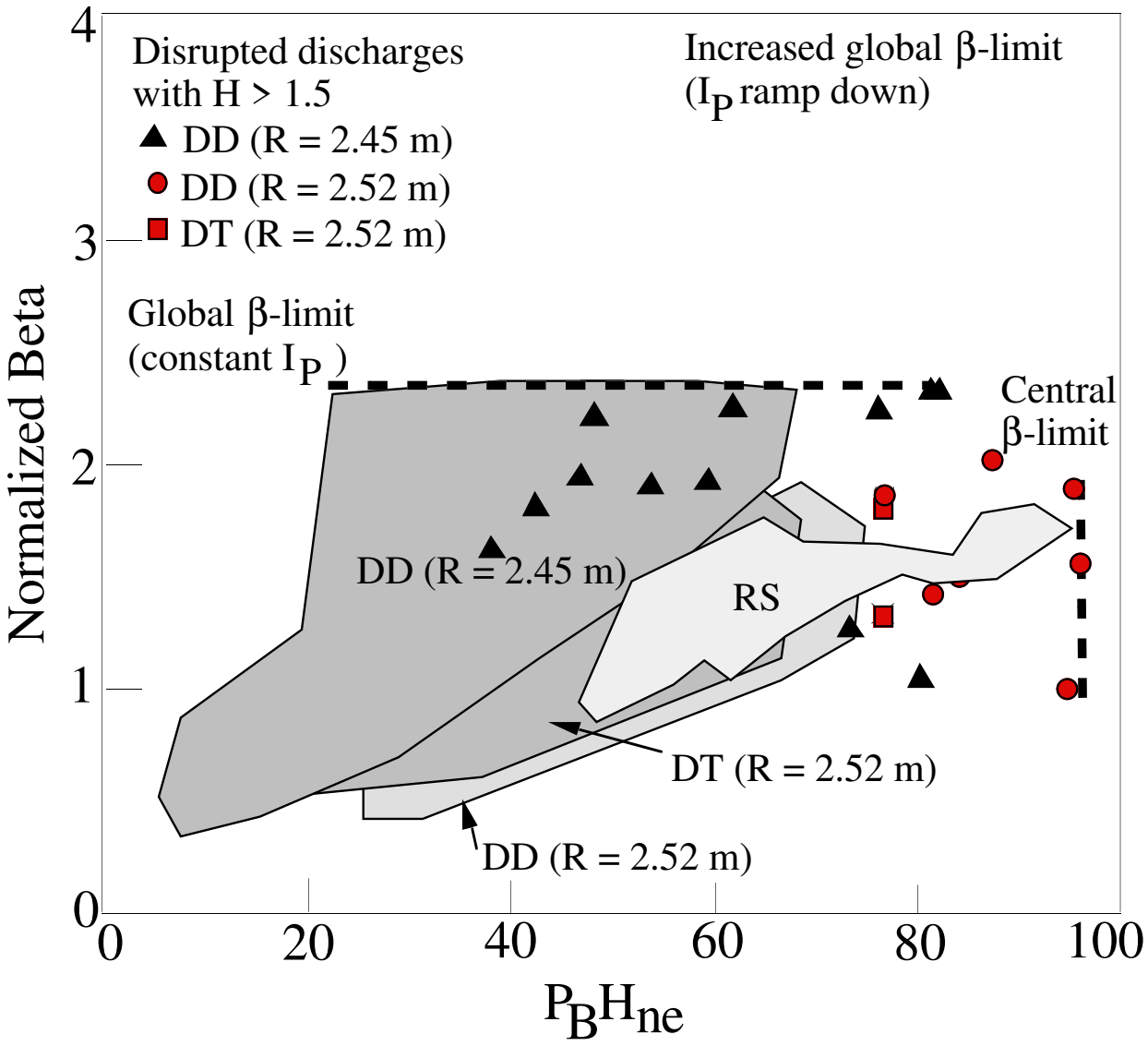
Disrupted discharges
with H > 1.5
DD (R = 2.45 m)
DD (R = 2.52 m)
DT (R = 2.52 m)
Increased global β-limit
(I_P ramp down)
Global β-limit
(constant I_P)
Central
β-limit
DD (R = 2.45 m)
RS
DT (R = 2.52 m)
DD (R = 2.52 m)
Normalized Beta
P_B H_ne
0
1
2
3
4
0
20
40
60
80
100

Fig 9

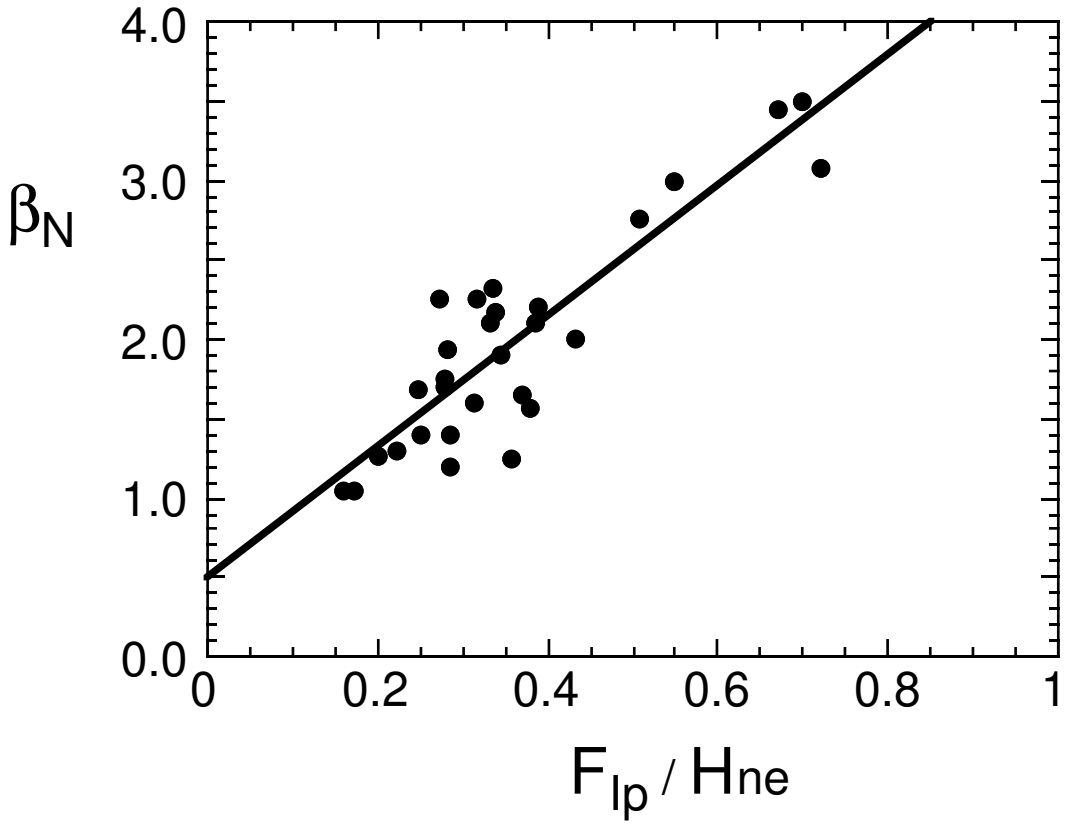

Fig. 10

Fig. 11

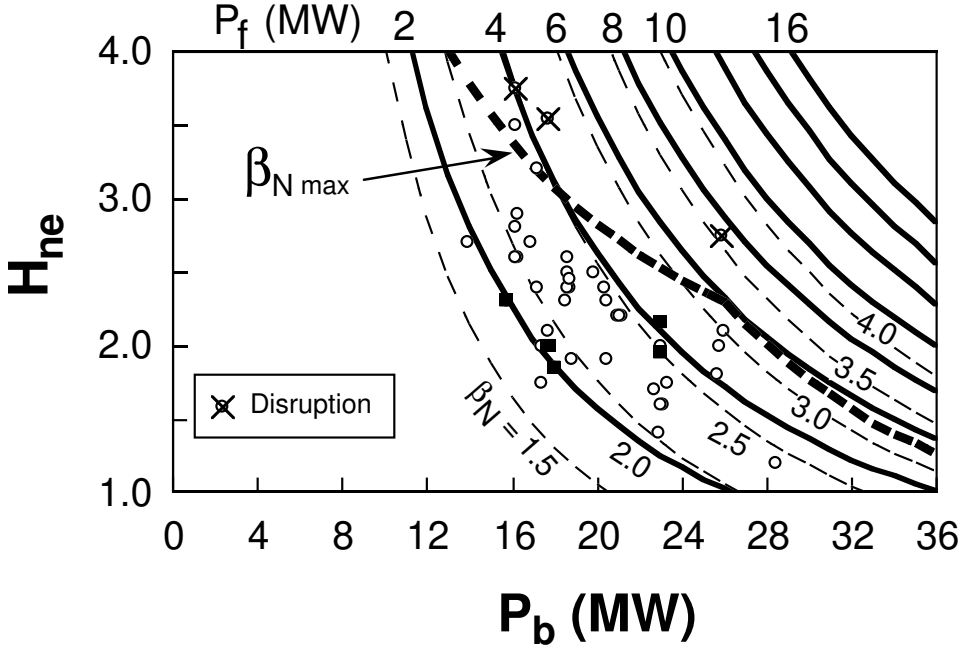
P_f (MW) 2 4 6 8 10 16
4.0
3.0
2.0
1.0
H_{ne}
$\beta_{N\,max}$
Disruption
β_N = 1.5
2.0
2.5
3.0
3.5
4.0
0 4 8 12 16 20 24 28 32 36
P_b (MW)

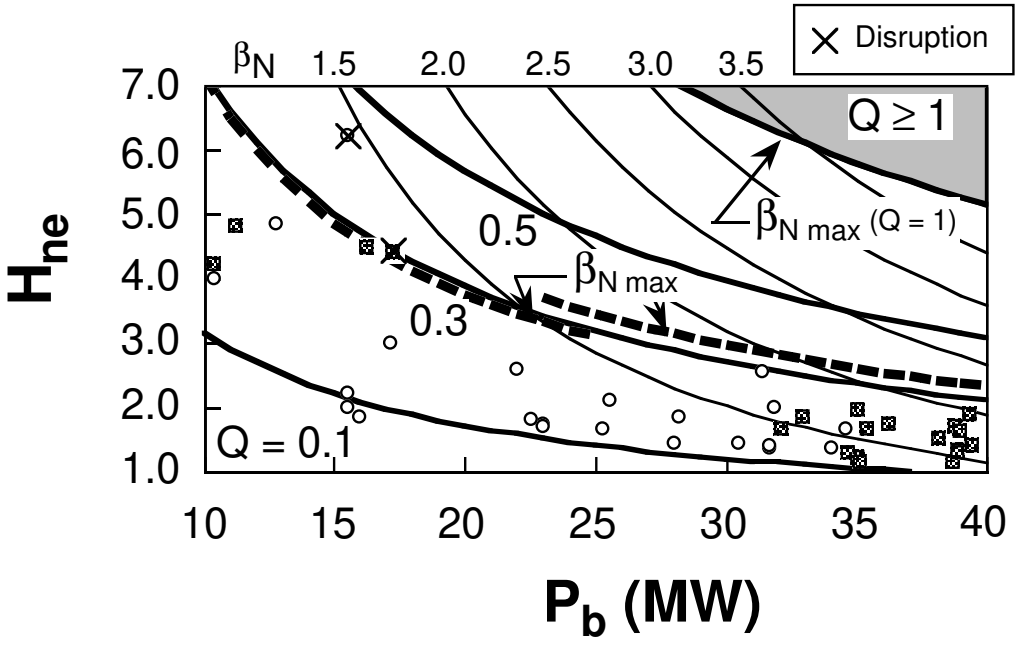
Disruption
β_N 1.5 2.0 2.5 3.0 3.5
7.0
6.0
5.0
4.0
3.0
2.0
1.0
H_{ne}
Q ≥ 1
$\beta_{N\,max}$ (Q = 1)
0.5
$\beta_{N\,max}$
0.3
Q = 0.1
10 15 20 25 30 35 40
P_b (MW)

Fig. 12